Chemical Science

ROYAL SOCIETY OF CHEMISTRY

EDGE ARTICLE

View Article Online
View Journal | View Issue

Cite this: *Chem. Sci.*, 2026, **17**, 2627

All publication charges for this article have been paid for by the Royal Society of Chemistry

Intramolecular transamidation enables one-pot synthesis of three chiral, Z-shaped perilenediimides for null-type supramolecular polymer formation

Alfonso J. Schwalb, Adrián Carreño, Fátima García and Luis Sánchez *

Building on the concept of null-type supramolecular polymers, we present herein the synthesis of three isomeric Z-shaped perylenediimides (Z-PDIs **1–3**), in which a central PDI core is linked to peripheral trisdodecyloxybenzamide groups by an alanine-derived linker. Interestingly, we discovered that both the starting amines used in the synthesis of symmetric Z-PDIs **1** and **3** can undergo intramolecular transamidation, allowing the one-pot generation of all three isomers **1–3**. The self-assembly behavior of these compounds was systematically explored using various spectroscopic methods. In line with our previous observations, the UV-Vis spectra of the aggregates closely resemble those of their monomeric forms, confirming the formation of null-type supramolecular polymers. Moreover, we found that the position of the stereogenic center strongly affects the aggregate stability: the assemblies become more stable when the stereocenter is positioned farther to the PDI core. The lateral benzamide groups facilitate kinetically controlled polymerization through the formation of intramolecular hydrogen-bonded pseudocycles, with the stereocenter's location again playing a key role in modulating the assembly kinetics. Finally, we demonstrate an efficient transfer of point chirality from the alanine-derived linker to the supramolecular structure, resulting in the formation of chiral null-type supramolecular polymers.

Received 23rd September 2025
Accepted 25th November 2025

DOI: 10.1039/d5sc07365k

rsc.li/chemical-science

Introduction

Jelley and Scheibe reported in 1936 and 1937, respectively and independently, the remarkable bathochromic shift observed in the absorption spectra and the increase in the emission intensity experienced by an aqueous solution of 1,1′-diethyl-2,2′-cyanine chloride in comparison to the absorption maxima observed for this compound in some other solvents.[1,2] They also reported the reversibility of these spectroscopic changes upon heating and cooling the dye solutions, which is diagnostic of an efficient self-assembly. The term J-type aggregates was coined based on these findings for those dye aggregates with an absorption band that is shifted to a longer wavelength in comparison to the monomeric species and an increase in the emission intensity.[3] On the other hand, it is also possible to observe the opposite effect when a dye self-assembles to form an aggregate, that is, the aggregation provokes a clear hypochromic effect accompanied by a depletion of the emission intensity in comparison to the monomeric species.[3] This is the case of H-type aggregates, following the Kasha's classification.[4] The optical response of dyes upon aggregation is related to the electronic communication between the chromophores, which, in turn, is conditioned by the π-overlap, the intermolecular distance, and the relative spatial orientation of the chromophores. In the above-mentioned Kasha's model,[4] the intermolecular interaction of the monomeric species is defined by the coulombic coupling (J_{Coul}) that stems from long-range electrostatic-like interactions. Exciton splitting and the corresponding shifts or divisions in absorption bands occur due to the interaction between transition dipoles in aggregated species. In addition to J-aggregates, which present a head-to-tail alignment of the chromophores, and H-aggregates, featuring a cofacial alignment of monomeric scaffolds, Kasha's exciton theory also predicts null-type aggregates showing no coulombic coupling due to specific dipole orientations.[4] Kasha's model of long-range coulombic coupling has been expanded to include short-range charge-transfer (CT) interactions, initially proposed by Harcourt, Scholes, and Ghiggino,[5] and later refined by Hestand and Spano,[6] who accounted for vibrational effects on the optical behavior of aggregates. These CT-based (J_{CT}) interactions arise from the overlap of the HOMO and LUMO orbitals in stacked chromophores and are highly dependent on the slip angle between monomer units. Consequently, categorizing aggregates solely as H- or J-type is overly simplistic and a more nuanced view that includes both CT and coulombic effects is necessary. In this context, null aggregates could be formed due to destructive interference between long-range and short-range interactions, along with a suitable energy offset between key low-lying excited states and should display spectral features similar to those of the individual monomers.[6] The seminal

Departamento de Química Orgánica, Facultad de Ciencias Químicas, Universidad Complutense de Madrid Ciudad Universitaria, 28040-Madrid, Spain. E-mail: lusamar@ucm.es

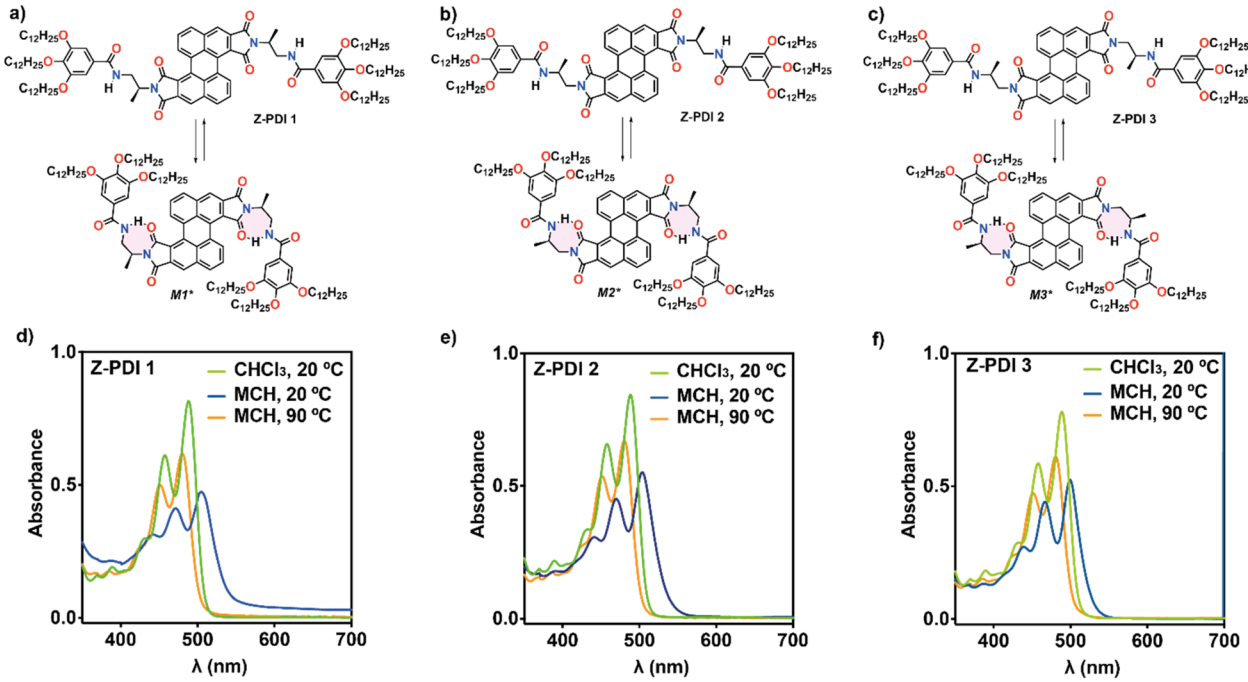

Fig. 1 (a–c) Chemical structure of chiral Z-PDIs **1–3** depicting the corresponding metastable monomeric species M* formed by intramolecular H-bonding interactions. (d–f) UV-Vis spectra of Z-PDIs **1–3** in $CHCl_3$ and MCH (c_T = 40 μM).

works by Jelley and Scheibe on J-type aggregates together with those reported by Aida's[7] and Lehn's[8] research groups paved the way to investigate the formation of a large number of aggregated species from different chromophores yielding supramolecular polymers with outstanding properties and applications.[9] These supramolecular polymers, in which chromophores like porphyrins,[10] oligomers,[11] 4,4-difluoro-4-bora-3a,4a-diaza-*s*-indacene (BODIPY) dyes,[12] rylenes,[13] and, especially, perylenediimides (PDIs),[14] are held together by non-covalent interactions,[15] are reported to form H- or J-type aggregates. However, the vast majority of the examples of null-type aggregates has been observed as crystalline samples, with the exception of PDI-based dimers and tetramers reported by Würthner and coworkers[16] and the oligogrids reported by Cao, Xie, and Guldi.[17,18] Nevertheless, very recently, we reported the formation of null-type supramolecular polymers in which the monomeric units are Z-shaped PDIs endowed with two lateral tris-dodecyloxybenzamide fragments. The supramolecular polymerization of this Z-shaped PDI in non-polar methylcyclohexane (MCH) solution gives rise to an aggregated species displaying an absorption pattern very similar, but slightly bathochromically shifted, to the monomeric species. Theoretical calculations have been crucial to further corroborate that, in these aggregates, both the coulombic J_{Coul} and the charge-transfer J_{CT} couplings are identical but of opposite sign which, unambiguously, indicate the formation of such null-type supramolecular polymers. Furthermore, these theoretical calculations reveal that these null-type aggregates are constituted by an arrangement of slipped monomeric units in which the lateral benzamide units interact by intermolecular H-bonds reinforced by the π-stacking of the central PDI moieties.[19]

Based on the description of this first example of a null-type supramolecular polymer, we report herein the synthesis of three isomeric Z-shaped perylenediimides (Z-PDIs **1–3**, Fig. 1), in which the central PDI core is connected to peripheral tris(alkoxy)benzamide units *via* an alanine-based linker. Notably, we found that the starting amines used to synthesize the symmetric Z-PDIs **1** and **3** can undergo a transamidation reaction, enabling the formation of all three isomers (Z-PDIs **1–3**) in a one-pot process. However, it is also possible to tune the conditions to bias the formation of only one isomer. The self-assembly behavior of these Z-PDIs was thoroughly investigated using various spectroscopic techniques. Consistent with our previous findings,[19] the UV-Vis spectra of the aggregated species of compounds **1–3** resemble those of the corresponding monomers, indicating the formation of null-type supramolecular polymers (Fig. 1d–f).

Furthermore, the position of the stereogenic center significantly influences the stability of the resulting aggregates: when the stereocenter is farther to the PDI core, the supramolecular assembly becomes more stable. The lateral benzamide units promote kinetically controlled polymerization through the formation of intramolecular hydrogen-bonded pseudocycles (Fig. 1a–c), with the stereocenter location again playing a decisive role in modulating the kinetics of self-assembly. Finally, we demonstrate the efficient transfer of point chirality from the alanine-derived linker to the supramolecular assemblies, yielding chiral null-type supramolecular polymers. The findings reported herein advance our understanding of null-type supramolecular polymer formation and open new avenues for accessing their chiral counterparts.

Results and discussion

Synthesis of the Z-PDIs 1–3 and transamidation experiments

The synthesis of the Z-PDI **1** was carried out by following a similar procedure to that previously reported for an *N*-annulated PDI in which the commercially available (*S*)-(+)-2-amino-1-propanol was the starting chiral reagent.[20] (*S*)-(+)-2-Amino-1-propanol was converted into benzamide **9** endowed with a free amine following a previously reported methodology (Scheme S1a).[21] The final reaction between dianhydride **10** with an excess of benzamide **9** (ref. 19) generated the corresponding imide functional groups. The synthesis of target Z-PDI **1** from benzamide **9** and dianhydride **10** was first attempted by heating this mixture in the presence of $Zn(AcO)_2$ and imidazole under microwave irradiation at 165 °C (Scheme 1, Method A, Scheme S2 and Entry 1 in Table 1), experimental conditions utilized for preparing the achiral Z-PDI previously reported by our group,[19] and many other PDI-based derivatives.[14,20,21] Upon removing the metallic salt residue and the imidazole, thin layer chromatography (TLC) of the reaction mixture revealed the presence of three greenish, highly emissive spots (Fig. S1a). To further analyze the chemical nature of these compounds, we obtained a HPLC chromatogram on a chiral stationary phase. This chromatogram shows three well defined peaks with retention times of 5.2, 6.5 and 7.9 min and with an absorption pattern characteristic of monomeric PDIs, diagnostic of the formation of three chiral Z-PDI isomers (Fig. S1b). Purification of the mixture by column chromatography allowed the isolation of these three chiral Z-PDIs whose mass spectra showed the same *m*/*z* value (see SI for details). The ^{1}H NMR spectra of the three

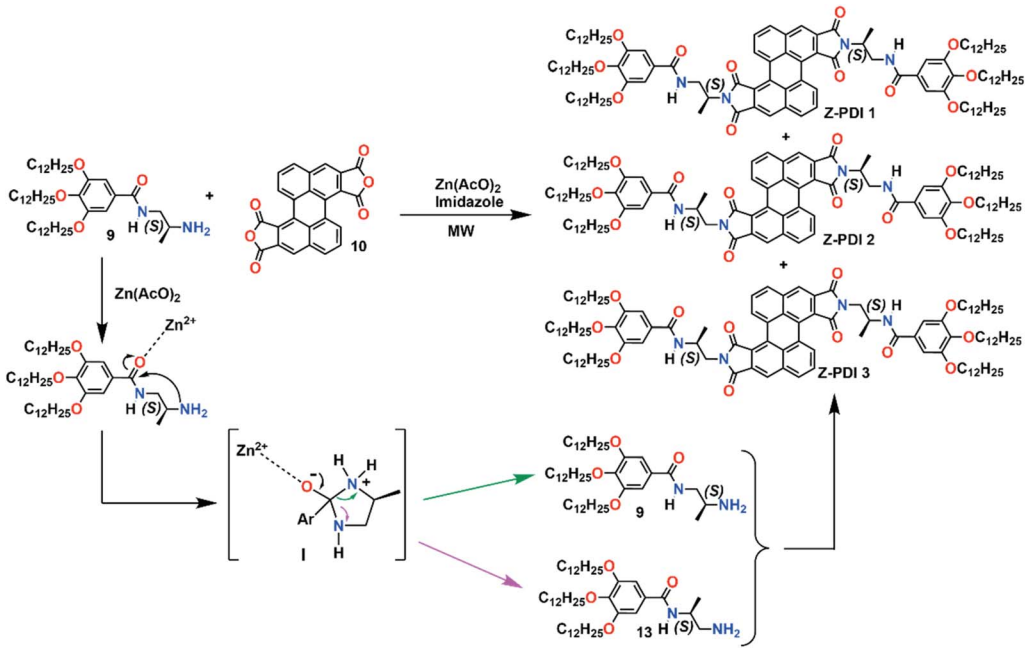

Scheme 1 Proposed Zn^{2+}-catalyzed intramolecular transamidation mechanism yielding a mixture of the three isomeric Z-PDIs **1**–**3**.

Table 1 Experimental reaction conditions utilized to convert benzamide **9** and dianhydride **10** into the Z-PDIs **1**–**3**

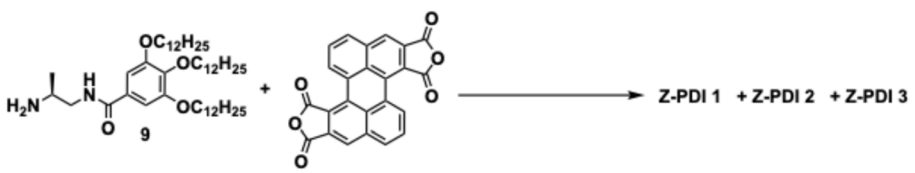

Entry	Temperature (°C)	$Zn(AcO)_2$	Solvent	Time (min)	% Z-PDI 1[a]	% Z-PDI 2[a]	% Z-PDI 3[a]	% Yield
1	165	Yes	Imidazole	40	30	50	20	43
2	165	Yes	*o*-DCB	40	34	51	15	31
3	165	No	Imidazole	40	77	18	5	21
4	110	Yes	Imidazole	40	84	12	4	19
5	110	No	Toluene	40	100	0	0	15
6	110	No	Toluene	180	100	0	0	27

[a] The ratio of the Z-PDIs has been derived from the peaks registered in the HPLC traces.

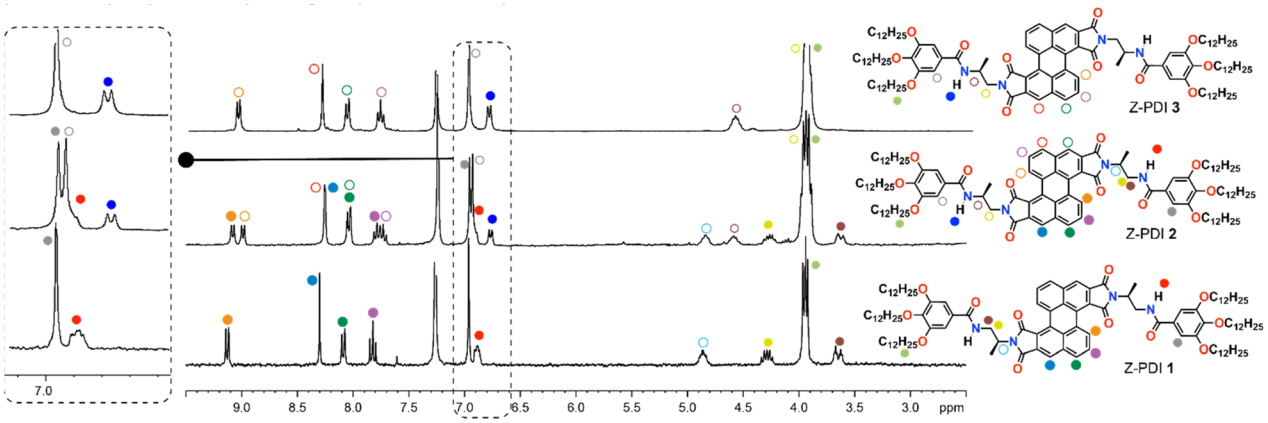

Fig. 2 Partial ^{1}H NMR spectra of Z-PDIs **1–3** showing the aromatic and part of the aliphatic protons. The left part of the panel depicts the zoomed in region of the amide protons (experimental conditions: $CDCl_3$; 298 K; 300 MHz).

isolated Z-PDIs in $CDCl_3$ contributed to the elucidation of the chemical structure of these isomeric compounds. The more polar Z-PDI showed a single set of resonances at δ ~7.8, 8.1, 8.3 and 9.15 (orange, light blue, green and purple circles in Fig. 2) corresponding to the aromatic protons of the Z-PDI core and a triplet at δ ~6.9 ascribable to the amide protons (red circle in Fig. 2). Furthermore, the multiplets observed at δ ~4.9, 4.4. and 4.2 are assigned to the alanine-derived linker and the multiplicity of the amide protons confirmed the formation of the expected Z-PDI **1** in which the stereogenic centers are located close to the imide functional groups.

In contrast, the ^{1}H NMR spectrum of the more apolar Z-PDI shows also a single set for the aromatic resonances at δ ~7.8, 8.1, 8.2 and 9.05 (orange, light blue, green and purple circles in Fig. 2) but the amide protons appear as a doublet at δ ~6.9 (blue circle in Fig. 2). This multiplicity implies that the sp^3 carbon adjacent to the NH of the peripheral benzamide unit possesses only one proton. These findings suggest the formation of Z-PDI **3** in which the stereogenic center is located at the outer carbon of the central linker thus involving a rearrangement of the starting benzamide **9**. The ^{1}H NMR spectrum of the Z-PDI of intermediate polarity presents a duplicate set of aromatic resonances coincident with the both above-mentioned Z-PDIs **1** and **3** with both the triplet and the doublet at δ ~6.9 and 6.8 ascribable to the NH of two different amide groups (red and blue circles, respectively, in Fig. 2). Apparently, this fraction could be assigned to an equimolecular mixture of both symmetric Z-PDIs **1** and **3**. However, the integral values are coincident with the formation of the asymmetric Z-PDI **2** in which the lateral linkers are different: in one of these side chains, the stereogenic center is closer to the central Z-PDI core, and, in the other one, this stereogenic center is farther to the central aromatic moiety (Fig. 2).

The formation of the three isomeric Z-PDIs **1–3** under these experimental conditions could be ascribed to a transamidation reaction,[22] a synthetic protocol previously described for the conversion of glutamine into pyrrolidinonecarboxylic acid,[23] or in the synthesis of diazepinones from β-lactams[24] but, to the best of our knowledge, never considered for the preparation of PDI-based scaffolds. To rationalize this transamidation reaction, we postulate that the Zn^{2+} cations play a crucial role. A large number of PDI derivatives are synthesized by using the Langhals' method, consisting of reacting perylene-3,4,9,10-tetracarcoxylic dianhydride with primary amines in molten imidazole, at 140–180 °C, and using zinc acetate as the catalyst. In this process, the Zn^{2+} cations are coordinated to the carbonyls of the starting dianhydrides to enhance their electrophilicity, thus favoring the nucleophilic attack of the amine group.[24] In our case, the coordination of the Zn^{2+} cations can also take place with the carbonyl of the benzamide group that can experience an intramolecular, nucleophilic attack of the free amine to yield an asymmetric, imidazolidinium intermediate (intermediate **I** in Scheme 1). Further opening of intermediate **I** gives rise to the initial benzamide **9** (green arrow) or to the isomeric benzamide **13** (pink arrow). The presence of both benzamides in the reaction mixture yields the three isomeric Z-PDIs **1–3** in a one-pot process (Scheme 1). In order to validate this hypothesis, we have performed different experiments. The first one involves the synthesis of tris(dodecyloxy)benzamide **13** starting from (*S*)-(+)-2-amino-1-propanol (Scheme S1b). The synthesis of amine **13** requires a multistep protocol consisting of the initial protection of the amino group of (*S*)-(+)-2-amino-1-propanol with *tert*-butyloxycarbonyl anhydride followed by a Mitsunobu S_N2 reaction of the alcohol **4** with phthalimide, DIAD and PPh_3 to yield compound **5**. The protected amine present in **5** was released by acidic hydrolysis to yield amine **11** that was reacted with 3,4,5-tris(dodecyloxy) benzoic acid **7** in the presence of EDC and DMAP to generate the amide **12**. The subsequent conversion of the imide present in **12** into the corresponding free amine was performed by treatment with hydrazine hydrate to afford benzamide **13**. The final reaction of this benzamide **13** with dianhydride **10** under the same conditions employed above (Method A, Scheme S2 and Entry 1 in Table 1) yielded the same mixture of three Z-PDIs **1–3**, as visualized in the TLC of the reaction mixture (Scheme S2 and Fig. S1c). Purification of these three compounds corroborates the formation of the Z-PDIs **1–3**.

To unravel the role of the imidazole, temperature and, especially, the role of the Zn^{2+} cations in the intramolecular

transamidation, we have carried out a series of reactions between benzamide **9** and dianhydride **10** modifying the experimental conditions (Table 1 and Fig. S2). Thus, if *ortho*-dichlorobenzene (*o*-DCB) is utilized as the solvent, adding $Zn(AcO)_2$ and heating the reaction mixture at 165 °C, a similar mixture of the three Z-PDIs is obtained (Entry 2 in Table 1 and Fig. S2). If imidazole is used as the solvent but without adding $Zn(AcO)_2$, the ratio between the three Z-PIDs **1**/**2**/**3** changes drastically being 77/18/5 (Entry 3 in Table 1 and Fig. S2). Decreasing the reaction temperature to 110 °C, with imidazole as the solvent and in the presence of $Zn(AcO)_2$, the **1**/**2**/**3** ratio is 84/12/4 (Entry 4 in Table 1 and Fig. S2). These data confirm that the best conditions to prevent the transamidation reaction is decreasing the reaction temperature and removing the $Zn(AcO)_2$ from the reaction. Thus, the use of toluene at 110 °C without adding $Zn(AcO)_2$ allows obtaining Z-PDI **1** as the only imide with increasing of the yield upon increasing the reaction time (Entrys 5 and 6 in Table 1, Fig. S2 and Method B, Scheme S3). This reaction takes place without the intramolecular transamidation reaction and either Z-PDI **1** or Z-PDI **3** can be exclusively obtained in higher yields using benzamide **9** or **13**, respectively (Method B, Scheme S3).

Chiral, null-type supramolecular polymers

Once the three isomeric Z-PDIs **1–3** were prepared, isolated and characterized, we investigated their self-assembly in solution. To elucidate the non-covalent forces operating in the supramolecular polymerization of Z-PDIs **1–3**, we have firstly registered ^{1}H NMR spectra in $CDCl_3$ at different concentrations. As for the previously reported achiral Z-PDI,[19] these concentration dependent studies show that all the aromatic resonances slightly shift upfield and the resonances corresponding to the amide protons deshield upon increasing the concentration for three chiral Z-PDIs **1–3** (Fig. 2). These shifts suggest the supramolecular interaction of these scaffolds by the formation of intermolecular H-bonds between the amide functional groups reinforced by the π-stacking of the central aromatic backbones. Noteworthily, these shifts are more pronounced for **1** than for **2** and **3** thus suggesting that the self-assembly of the symmetric Z-PDI **1** is more favorable than those of Z-PDIs **2** and **3**. The formation of the intermolecular H-bonding interactions has been corroborated by registering FTIR spectra in non-polar solvent MCH. The NH stretching band of **1–3** in MCH appears as a single band at 3268, 3289 and 3291 cm^{-1}, respectively, wavenumber values ascribable to intermolecular H-bonding interactions (Fig. 3a and S4).[19,21] The formation of such intermolecular H-bonding interactions between the amide functional groups of **1–3** is confirmed by the amide I band that appears at 1635, 1639 and 1641 cm^{-1}, respectively.[19,21] These wavenumber values observed for **1–3** in MCH contrast with those registered in chloroform, a good solvent that favors the disassembly of the aggregates.[25,26] In this good solvent, the NH and amide I stretching bands are observed at 3448 and 1652 cm^{-1}, respectively, values that have been ascribed to free amides (Fig. 3a and S4).[19,21] It is worth mentioning that, additionally, the FTIR spectra of **1–3** in the good solvent $CHCl_3$ also present an additional band at ~3415 cm^{-1} that is diagnostic of the presence of intramolecular H-bonding interactions formed between the NH of the peripheral benzamide and one of the carbonyls of the imide functional groups (Fig. 3a and S4).[19,21] These intramolecular H-bonding interactions have been also detected by registering the ^{1}H NMR spectra of Z-PDIs **1–3** in $CDCl_3$ at a total concentration $c_T = 1$ mM at different temperatures. In these variable temperature (VT) ^{1}H NMR spectra, increasing the temperature provokes a shielding effect on the resonances ascribable to the NH of the amide functional groups due to the rupture of such intramolecular H-bonding interactions. However, under these conditions, the π-stacking of the aromatic moieties is not present since increasing the temperature is not accompanied by the shift of any aromatic resonances, except the protons at the bay positions due to the proximity of the tris(alkoxy)benzamide fragment upon forming the seven-membered pseudocycles (orange circles in Fig. 3b and S5).

Our previous results on the supramolecular polymerization of an achiral Z-PDI in MCH reveal the formation of null-type

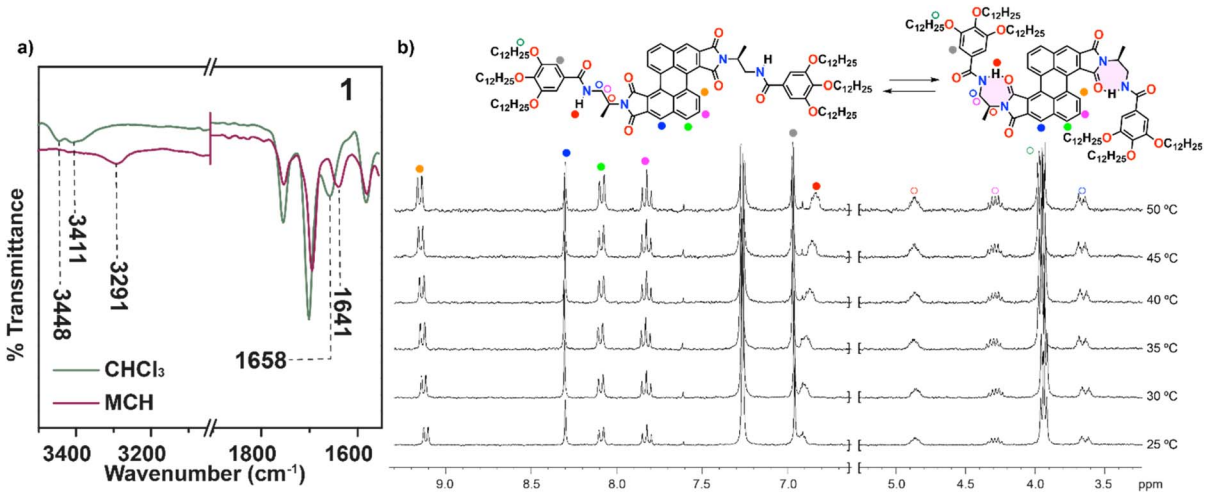

Fig. 3 Partial FTIR (a) and VT-1H NMR spectra (b) of Z-shaped PDIs **1** showing the stretching NH and amide I bands (a) and the aromatic and part of the aliphatic protons (b) (Experimental conditions: $c_T = 1$ mM; $CDCl_3$; 298 K; 300 MHz for panel (b)).

aggregates characterized by an absorption pattern coincident in shape with that registered for the monomeric species but slightly red-shifted. The formation of such null aggregates has been unambiguously confirmed by extensive theoretical calculations.[19] In the case of the studied Z-PDIs **1–3**, the UV-Vis spectra in both the good solvent $CHCl_3$, which favors a molecularly dissolved state, and in the poor solvent MCH, which strongly favors self-assembly, show an identical pattern to that registered for the previously reported Z-PDI. Thus, the UV-Vis spectra of **1–3** show maxima centered at $\lambda = 481$ and 455 nm and a shoulder at $\lambda = 426$ nm, ascribable to the characteristic vibronic A_{0-0}, A_{0-1} and A_{0-2} transitions of the lowest energy electronic transition of perylene-based scaffolds in their monomeric state (Fig. 1d–f and 4d–f).[19,27] In MCH at 20 °C, these UV-Vis spectra present an identical pattern with absorption maxima at $\lambda = 500$ and 466 nm and a shoulder at $\lambda = 434$ nm (Fig. 1d–f and 4d–f). This red-shift in the absorption maxima has been ascribed to the formation of null-type aggregates in which the adjacent monomeric species interact by intermolecular H-bonds between the amide functional groups, and the central aromatic moieties adopt a ladder-like arrangement separated by 3.5 Å.[19] Heating up these solutions of Z-PDIs **1–3** in MCH to 90 °C provokes the disassembly of the corresponding aggregates as demonstrated by the blue-shift of the absorption maxima that appear centered at $\lambda = 479$ and 450 nm and a shoulder at $\lambda = 422$ nm (Fig. 1d–f).

The above-mentioned FTIR and VT-^{1}H NMR spectra, and the previous results on the achiral Z-PDI, indicate that the supramolecular polymerization of the Z-PDIs **1–3** could be a kinetically controlled process due to the formation of the metastable pseudocycles M1*–M3* (Fig. 1a–c). To confirm this statement, we have registered the variation of the absorption pattern of diluted solutions of Z-PDIs **1–3** in MCH with the temperature both in cooling and heating process (Fig. S6). The resulting cooling and heating curves, obtained upon plotting the variation of the absorption at $\lambda = 481$ nm, reveal a clear hysteresis, diagnostic of the formation of the pseudocycles M1*–M3* (Fig. 4a–c).[19,28]

These cooling/heating cycles show two interesting features of the aggregates formed by the supramolecular polymerization of **1–3**. Thus, the temperature of elongation (T_e), that is, the temperature at which the small nuclei formed initially grow to form the final supramolecular polymers,[15a] for the symmetric Z-PDI **3** with the stereogenic centers farther to the aromatic moiety, is much higher than that registered for the symmetric Z-PDI **1**, with the stereogenic centers closer to the aromatic moiety ($T_{e3} = 88$ °C *vs.* $T_{e1} \sim 10$ °C in the cooling process; Fig. 4a–c). Interestingly, the T_e of asymmetric Z-PDI **2** presents an intermediate value of 54 °C. These T_e values clearly indicate that the stability of the null type aggregates is directly related to the position of the stereogenic centers at the central tethers. Furthermore, the cooling/heating cycles also reveal that the kinetics of the process is much slower in the case of Z-PDI **1** since the absorption maximum of the null type supramolecular polymers formed from this Z-PDI in the cooling process is blue-shifted in comparison to the absorption maximum observed for **3** in the heating process or the other two Z-PDIs **2** and **3** ($\lambda_{max} =$ 479 nm *vs.* $\lambda_{max} = 505$ nm, Fig. S6). The hysteresis observed in the cooling/heating cycles prevents an accurate determination of the stability of the supramolecular polymers formed by **1–3** by applying the one-component equilibrium model to the VT-UV-Vis experiments.[29] However, the application of the solvent denaturation (SD) model allows deriving the Gibbs free energy, the degree of cooperativity σ and the parameter m that indicates the influence of the good solvent on the stability of the supramolecular polymers (Fig. 4d–f).[26] In the SD experiments, the UV-Vis spectra of mixtures of solutions of Z-PDIs **1–3** at different ratios of the good solvent $CHCl_3$ and the poor solvent MCH, while keeping constant the total concentration, are registered. Plotting the degree of aggregation α (calculated from the absorption at $\lambda = 481$ nm for both the monomeric and aggregated states)[14a] *versus* the molar fraction of $CHCl_3$ yields non-sigmoidal curves for the three studied Z-PDIs diagnostic of a cooperative process (Fig. 4g–i).[15a] The derived thermodynamic parameters are collected in Table 2 and show the higher stability of the aggregates formed by Z-PDI **3** in comparison to those formed by **1** and **2**. In addition, the degree of cooperativity is also higher for **3** than **1** and **2**, as revealed by the derived σ parameter (Table 2).

The morphology of the supramolecular polymers formed by Z-PDIs **1–3** in MCH has been visualized by atomic force microscopy (AFM) imaging onto highly oriented pyrolytic graphite (HOPG) as the surface. In all cases, the null-type aggregates formed by these Z-PDIs appear in the AFM images as long, rope-like fibers (Fig. S7). The presence of the stereogenic center in the central tether of the studied systems makes compounds **1–3** chiral scaffolds in which the point chirality embedded in the lateral linkers can be transferred in the self-assembly process giving rise to chiral, null-type aggregates.[29] To investigate this transfer of asymmetry from the monomeric to the thermodynamically controlled aggregated species, we have registered the corresponding circular dichroism (CD) spectra under different experimental conditions.[30] The CD spectra of the monomeric species, obtained in chloroform or in MCH at 90 °C, show a residual dichroic signal at $\lambda \sim 300$ nm (Fig. S8). However, the aggregated species of the three Z-PDIs **1–3**, registered in MCH at 20 °C, display a negative, monosignated CD spectra, with maxima at $\lambda \sim 425$ and 465 nm and a shoulder at $\lambda \sim 500$ nm, characteristic of an off-resonance coupling between the transition dipoles and resembling those reported for chiral J-type aggregates formed by PDI-based self-assembling units (Fig. 5a and S8).[31,32] This pattern contrasts with the bisignated dichroic pattern reported for H-type aggregated species formed by chiral PDIs.[32c,33]

Finally, we have complemented the study of the chiroptical properties of Z-PDIs **1–3** by registering the emission and circularly polarized (CPL) spectra (Fig. S9). In good analogy of the null-type aggregates formed by the achiral congener previously reported,[19] the photoluminescence (PL) spectra present a broad band centered at $\lambda = 555$ nm for **1** and $\lambda = 540$ nm for **2** and **3** (Fig. S9). Regarding the CPL activity of the supramolecular polymers formed by **1–3**, while the monomeric species do not exhibit CPL activity, the aggregated Z-PDIs present weak CPL activity with a dissymmetry factor $g_{lum} \sim 0.001$ and a negative

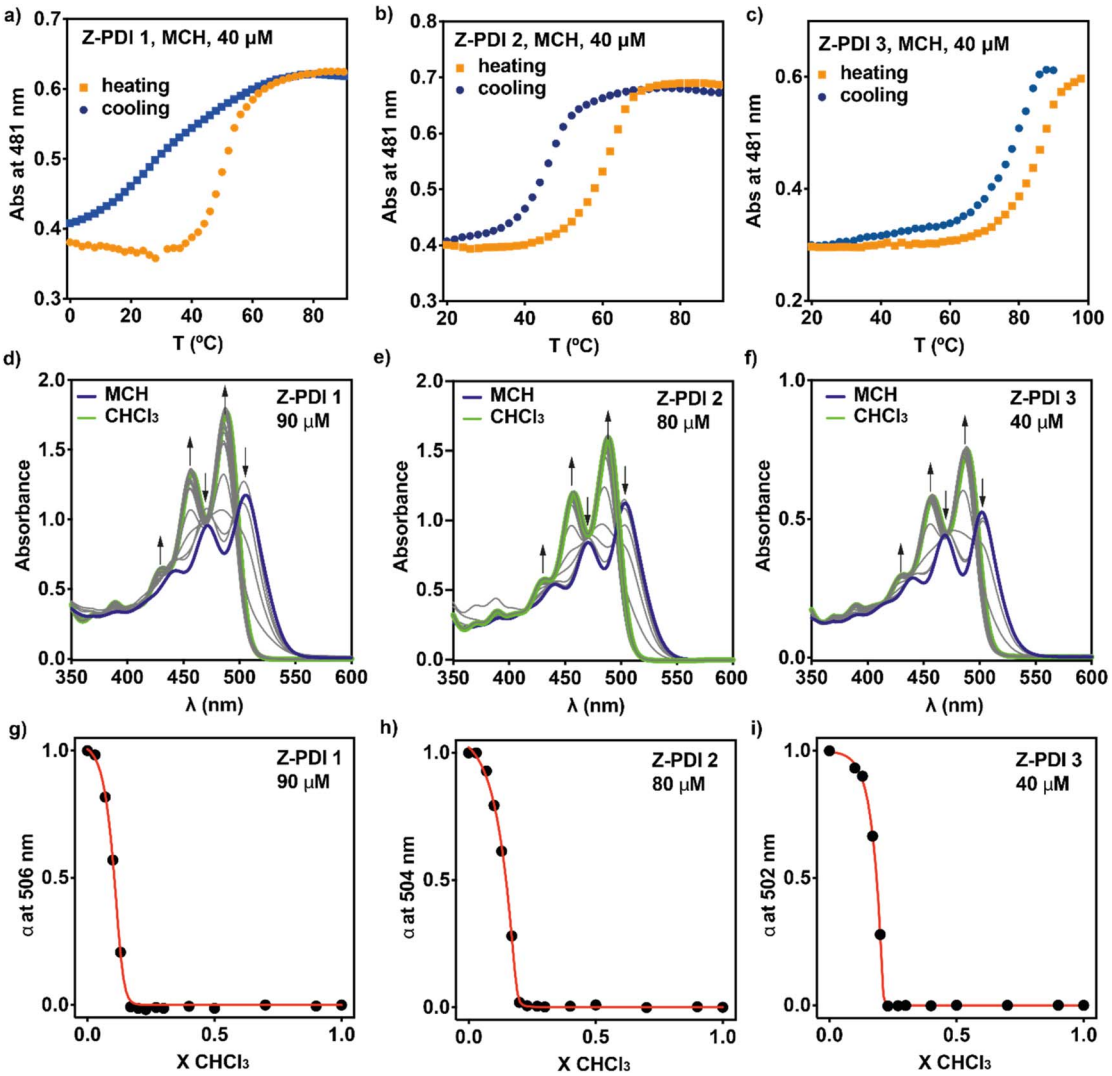

Fig. 4 (a–c) Cooling and heating curves of **1**–**3** in MCH upon applying a cooling/heating rate of 1 °C min^{-1}. (d–f) UV-Vis spectra of **1** (d), **2** (e) and **3** (f) in different MCH/$CHCl_3$ ratios. Arrows indicate the changes in the absorption pattern upon increasing the amount of $CHCl_3$. (g–i) Plot of the variation of the degree of aggregation α *versus* the molar fraction of $CHCl_3$. The red line depicts the fitting to the SD model[26] ($c_T = 90$ μM for **1**, 80 μM for **2** and 40 μM for **3**).

Table 2 Thermodynamic parameters associated with the cooperative supramolecular polymerization mechanism of compounds **1**–**3** at 298 K

Compound	$\Delta G'$ (kJ·mol^{-1})	m (–)	σ (–)
Z-PDI **1**	−29.5 ± 1	51	1.3×10^{-3}
Z-PDI **2**	−29.9 ± 1	47	1.3×10^{-3}
Z-PDI **3**	−38.2 ± 7	64	6.9×10^{-5}

signal for the three supramolecular polymers (Fig. S9), in agreement with the dichroic signals obtained (Fig. S8).

Pathway complexity for Z-PDI 1

Finally, we have investigated the kinetics of the supramolecular polymerization of Z-PDI **1** since this Z-PDI presents the higher hysteresis in the heating/cooling curves (Fig. 4a). The UV-Vis spectra of Z-PDI **1** in MCH registered in the cooling experiment demonstrate the complete disassembly of the aggregated species to afford the monomeric species upon heating up to 90 °C. Cooling down this MCH solution to 0 °C results in an absorption pattern different to that registered for Z-PDIs **1**–**3** at room temperature and ascribable to the null-type supramolecular polymers. In this case, the absorption pattern presents maxima at $\lambda = 497$ and 474 nm, the last being the most intense band (green spectrum in Fig. 5b). Interestingly, the CD spectrum of this species displays a positive monosignated pattern that is a mirror image of the CD registered for the thermodynamically controlled supramolecular polymer (Fig. 5b). Furthermore, the morphology of the kinetically controlled aggregated species AggI is very different to that observed for the null-type supramolecular polymers formed from **3** (AggII). Thus, the AFM images of this AggI species present a globular appearance (Fig. S10). To further investigate the kinetics of the

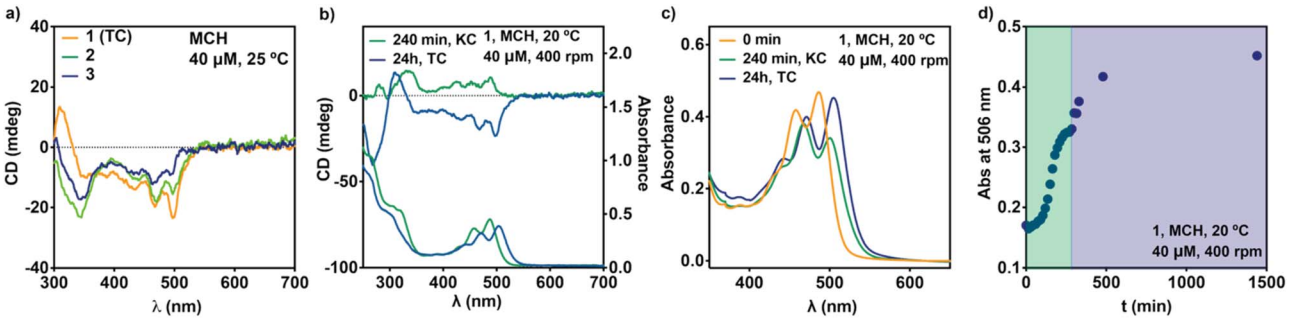

Fig. 5 (a) CD spectra of the thermodynamically controlled null-type aggregates formed by Z-PDIs **1–3**; (b) CD spectra of the kinetically (green line) and thermodynamically controlled (blue line) aggregated species of Z-PDI **1** in MCH; (c) UV spectra of Z-PDI **1** at different times; (d) kinetic profile showing the evolution of the maximum at $\lambda = 506$ nm in which the two regimes are shown in green and blue. Experimental conditions: solvent: MCH; $c_T = 40$ μM.

self-assembly process of **1**, we have registered a kinetic profile by monitoring the changes in the absorption at $\lambda = 506$ nm, wavelength characteristic of the thermodynamically controlled aggregated formed by **1**. To register this change, we have prepared a solution of **3** in MCH at $c_T = 40$ μM, heated this solution up to 90 °C to complete the disassembly of the aggregated species, and cooled it down rapidly to 20 °C. This solution presents the absorption pattern of the monomeric species (Fig. 5c). We have detected that keeping this solution at 20 °C results in a very slow conversion into the aggregated species. Therefore, to accelerate the conversion, we have applied mechanical stirring at 400 rpm. Under these conditions, the monomeric species evolve in 240 min to AggI, as demonstrated by the corresponding absorption pattern (Fig. 5c). Furthermore, the kinetic profile follows a sigmoidal shape, diagnostic of an autocatalytic transformation (Fig. 5d). Finally, upon applying these experimental conditions, we have observed the gradual conversion of the kinetically controlled aggregated species to the thermodynamically controlled null type supramolecular polymers AggII and it is completed in 24 hours. This stepwise monomer → AggI → AggII transformation suggests a consecutive conversion in which the AggI species are not disassembled to the monomers that, later on, are transformed into AggII.[34]

Finally, we have also checked the CPL-activity of the kinetically controlled AggI species. In this case, despite the weak CPL activity, the signal is of opposite sign to that registered for the AggII species (Fig. S9b), also in agreement with the dichroic signal obtained (Fig. S8).

Conclusions

Expanding on the concept of null-type supramolecular polymers, we report herein the synthesis of three isomeric Z-shaped perylenediimides (Z-PDIs **1–3**), featuring a central PDI core connected to peripheral tris(dodecyl)oxybenzamide units *via* an alanine-based linker. Notably, the symmetric Z-PDIs **1** and **3** are derived from starting amines capable of undergoing intramolecular transamidation, enabling the efficient, one-pot synthesis of all three isomers. The self-assembly behavior of these Z-PDIs, which takes place by the operation of intermolecular H-bonding interactions between the amide functional groups and the π-stacking of the central PDI cores, was comprehensively characterized using a range of spectroscopic techniques. Consistent with our earlier findings on null-type supramolecular polymers, the UV-Vis spectra of the aggregated species closely mirror those of the corresponding monomers, supporting the formation of null-type supramolecular polymers. Importantly, the spatial placement of the stereogenic center was found to significantly influence aggregate stability: increased separation from the PDI core correlates with enhanced structural stability. The peripheral benzamide moieties promote kinetically controlled polymerization through the formation of intramolecular hydrogen-bonded pseudocycles, with the stereocenter's position again playing a critical role in modulating the kinetics of self-assembly. Finally, we demonstrate the effective transmission of point chirality from the molecular linker to the supramolecular architecture, yielding chiral, null-type supramolecular polymers. These results deepen our understanding of null-type polymer systems and open new avenues for the design of their chiral analogues.

Author contributions

Alfonso J. Schwalb and Adrián Carreño: synthesis of the Z-PDIs, in-solution studies, AFM imaging, and writing; Fátima García and Luis Sánchez: conceptualization, writing, supervision, and funding acquisition.

Conflicts of interest

There are no conflicts to declare.

Data availability

The data that support the findings of this study have been included in the main text and supplementary information (SI) and are available from the corresponding authors upon reasonable request. Supplementary information: experimental procedures, spectroscopic characterization and additional figures. See DOI: https://doi.org/10.1039/d5sc07365k.

Acknowledgements

Financial support from the MICIU/AEI of Spain (PID2023-146971NB-I00 and CNS2022-136058) is acknowledged.

Notes and references

1 (*a*) G. Scheibe, *Angew. Chem.*, 1937, **50**, 51; (*b*) G. Scheibe, L. Kandler and H. Ecker, *Naturwissenschaften*, 1937, **25**, 75; (*c*) G. Scheibe, *Angew. Chem.*, 1937, **50**, 212; (*d*) G. Scheibe, *Angew. Chem.*, 1936, **49**, 563.

2 (*a*) E. E. Jelley, *Nature*, 1936, **138**, 1009; (*b*) E. E. Jelley, *Nature*, 1937, **139**, 631.

3 F. Würthner, T. E. Kaiser and C. R. Saha-Möller, *Angew. Chem., Int. Ed.*, 2011, **50**, 3376.

4 (*a*) M. Kasha, H. R. Rawls and M. A. El-Bayoumi, *Pure Appl. Chem.*, 1965, **11**, 371–392; (*b*) A. S. Davydov, *Phys. Usp.*, 1964, **7**, 145.

5 R. D. Harcourt, G. D. Scholes and K. P. Ghiggino, *J. Chem. Phys.*, 1994, **101**, 10521.

6 N. J. Hestand and F. C. Spano, *Acc. Chem. Res.*, 2017, **50**, 341.

7 T. Aida, A. Takemura, M. Fuse and S. Inoue, *J. Chem. Soc., Chem. Commun.*, 1988, 391.

8 C. Fouquey, J.-M. Lehn and A.-M. Levelut, *Adv. Mater.*, 1990, **2**, 254.

9 (*a*) Z. Álvarez, A. N. Kolberg-Edelbrock, I. R. Sasselli, J. A. Ortega, R. Qiu, Z. Syrgiannis, P. A. Mirau, F. Chen, S. M. Chin, S. Weigand, E. Kiskinis and S. I. Stupp, *Science*, 2021, **374**, 848; (*b*) R. P. Sijbesma, F. H. Beijer, L. Brunsveld, B. J. B. Folmer, K. J. H. K. Hirschberg, R. F. M. Lange, J. K. L. Lowe and E. W. Meijer, *Science*, 1997, **278**, 1601; (*c*) O. Dumele, L. Đordevic, H. Sai, T. J. Cotey, M. H. Sangji, K. Sato, A. J. Dannenhoffer and S. I. Stupp, *J. Am. Chem. Soc.*, 2022, **144**, 3127; (*d*) W. Zhao, J. Tropp, B. Qiao, M. Pink, J. D. Azoulay and A. H. Flood, *J. Am. Chem. Soc.*, 2020, **142**, 2579; (*e*) Y. Yanagisawa, Y. Nan, K. Okuro and T. Aida, *Science*, 2018, **359**, 72.

10 (*a*) J.-H. Fuhrhop, C. Demoulin, C. Boettcher, J. Köning and U. Siggel, *J. Am. Chem. Soc.*, 1992, **114**, 4159; (*b*) F. Helmich, C. M. Lee, M. M. L. Nieuwenhuizen, J. C. Gielen, P. C. M. Christianen, A. Larsen, G. Fytas, P. E. L. G. Leclére, A. P. H. J. Schenning and E. W. Meijer, *Angew. Chem., Int. Ed.*, 2010, **49**, 3939; (*c*) S. Ogi, K. Sugiyasu, S. Manna, S. Samitsu and M. Takeuchi, *Nat. Chem.*, 2014, **6**, 188.

11 (*a*) P. Jonkheijm, P. van der Schoot, A. P. H. J. Schenning and E. W. Meijer, *Science*, 2006, **313**, 80; (*b*) E. E. Greciano, J. Calbo, J. Buendía, J. Cerdá, J. Aragó, E. Ortí and L. Sánchez, *J. Am. Chem. Soc.*, 2019, **141**, 7463.

12 (*a*) Z. Chen, Y. Liu, W. Wagner, V. Stepanenko, X. Ren, S. Ogi and F. Würthner, *Angew. Chem., Int. Ed.*, 2017, **56**, 5729; (*b*) A. Sampedro, A. Ramos-Torres, C. Schwöppe, C. Mück-Lichtenfeld, I. Helmers, A. Bort, I. Díaz-Laviada and G. Fernández, *Angew. Chem., Int. Ed.*, 2018, **57**, 17235.

13 (*a*) A. Sikder, D. Ray, V. K. Aswal and S. Ghosh, *Angew. Chem., Int. Ed.*, 2019, **58**, 1606; (*b*) B. Mahlmeister, T. Schembri, V. Stepanenko, K. Shoyama, M. Stolte and F. Würthner, *J. Am. Chem. Soc.*, 2023, **145**, 13302.

14 (*a*) J. van Herrikhuyzen, A. Syamakumari, A. P. H. J. Schenning and E. W. Meijer, *J. Am. Chem. Soc.*, 2004, **126**, 10021; (*b*) S. Ghosh, X.-Q. Li, V. Stepanenko and F. Würthner, *Chem.–Eur J.*, 2008, **14**, 11343; (*c*) A. J. Schwalb, F. García and L. Sánchez, *Chem. Sci.*, 2024, **15**, 8137.

15 (*a*) T. F. A. De Greef, M. M. J. Smulders, M. Wolffs, A. P. H. J. Schenning, R. P. Sijbesma and E. W. Meijer, *Chem. Rev.*, 2009, **109**, 5687; (*b*) M. Wehner and F. Würthner, *Nat. Rev. Chem.*, 2020, **4**, 38.

16 (*a*) C. Kaufmann, D. Bialas, M. Stolte and F. Würthner, *J. Am. Chem. Soc.*, 2018, **140**, 9986; (*b*) L. Ernst, H. Song, D. Kim and F. Würthner, *Nat. Chem.*, 2025, **17**, 767.

17 Y. Bo, P. Hou, J. Wan, H. Cao, Y. Liu, L. Xie and D. M. Guldi, *Adv. Mater.*, 2023, **35**, 2302664.

18 (*a*) Z. Xie, B. Yang, F. Li, G. Cheng, L. Liu, G. Yang, H. Xu, L. Ye, M. Hanif, S. Liu, D. Ma and Y. Ma, *J. Am. Chem. Soc.*, 2005, **127**, 14152; (*b*) N. Sanyal and P. M. Lahti, *Cryst. Growth Des.*, 2006, **6**, 1253; (*c*) B. Zhang, H. Soleimaninejad, D. J. Jones, J. M. White, K. P. Ghiggino, T. A. Smith and W. W. H. Wong, *Chem. Mater.*, 2017, **29**, 8395; (*d*) E. Sebastian, A. M. Philip, A. Benny and M. Hariharan, *Angew. Chem., Int. Ed.*, 2018, **57**, 15696.

19 A. J. Schwalb, C. Naranjo, A. Fernández-Alarcón, F. García, E. Ortí, J. Aragó and L. Sánchez, *J. Am. Chem. Soc.*, 2025, **147**, 25024.

20 C. Naranjo, A. Doncel-Giménez, R. Gómez, J. Aragó, E. Ortí and L. Sánchez, *Chem. Sci.*, 2023, **14**, 9900.

21 M. Wehner, M. I. S. Röhr, M. Bühler, V. Stepanenko, W. Wagner and F. Würthner, *J. Am. Chem. Soc.*, 2019, **141**, 6092.

22 M. E. González-Rosende, E. Castillo, J. Lasri and J. Sepúlveda-Arques, *Prog. React. Kinet. Mech.*, 2004, **29**, 311.

23 R. B. Artin, A. Parcell and R. I. Hedrick, *J. Am. Chem. Soc.*, 1964, **86**, 2406.

24 A. Vasudevan, C. I. Villamil and S. W. Djuric, *Org. Lett.*, 2004, **6**, 3361.

25 (*a*) H. Langhals, *Chem. Ber.*, 1985, **118**, 4641; (*b*) H. Langhals, *Heterocycles*, 1995, **40**, 477.

26 (*a*) P. A. Korevaar, C. Schaefer, T. F. A. de Greef and E. W. Meijer, *J. Am. Chem. Soc.*, 2012, **134**, 13482; (*b*) L. López-Gandul, C. Naranjo, C. Sánchez, R. Rodríguez, R. Gómez, J. Crassous and L. Sánchez, *Chem. Sci.*, 2022, **13**, 11577.

27 F. Würthner, C. R. Saha-Möller, B. Fimmel, S. Ogi, P. Leowanawat and D. Schmidt, *Chem. Rev.*, 2016, **116**, 962.

28 S. Ogi, V. Stepanenko, K. Sugiyasu, M. Takeuchi and F. Würthner, *J. Am. Chem. Soc.*, 2015, **137**, 3300.

29 H. M. M. ten Eikelder, A. J. Markvoort, T. F. A. de Greef and T. P. A. J. Hilbers, *J. Phys. Chem. B*, 2012, **116**, 5291.

30 F. García, R. Gómez and L. Sánchez, *Chem. Soc. Rev.*, 2023, **52**, 7524.

31 N. S. S. Nizar, M. Sujith, K. Swathi, C. Sissa, A. Painelli and K. G. Thomas, *Chem. Soc. Rev.*, 2021, **50**, 11208.

32 (*a*) S. Ghosh, X.-Q. Li, V. Stepanenko and F. Würthner, *Chem.–Eur. J.*, 2008, **14**, 11343; (*b*) F. Würthner, C. Bauer, V. Stepanenko and S. Yagai, *Adv. Mater.*, 2008, **20**, 1695; (*c*) M. A. Martínez, A. Doncel-Gimenez, J. Cerdá, J. Calbo, R. Rodríguez, J. Aragó, J. Crassous, E. Ortí and L. Sánchez, *J. Am. Chem. Soc.*, 2021, **143**, 13281.

33 (*a*) Y. Huang, J. Hu, W. Kuang, Z. Wei and C. F. J. Faul, *Chem. Commun.*, 2011, **47**, 5554; (*b*) D. Hartmann, S. E. Penty, M. A. Zwijnenburg, R. Pal and T. A. Barendt, *Angew. Chem., Int. Ed.*, 2025, **64**, e202501122.

34 J. Matern, Y. Dorca, L. Sánchez and G. Fernández, *Angew. Chem., Int. Ed.*, 2019, **58**, 16730.